PAPER

CrossMark
click for updates

Adjusting the band structure and defects of ZnO quantum dots *via* tin doping†

Weimin Yang,[ab] Bing Zhang,[ab] Qitu Zhang,*[ab] Lixi Wang,[ab] Bo Song,[c] Yong Ding[c] and C. P. Wong[cd]

The structures and band structures of Sn doped ZnO were investigated by density functional theory (DFT). Sn-doped ZnO quantum dots were also synthesized *via* an ultrasonic sol−gel method. The charge of Sn ions was also taken into consideration and Sn^{2+} and Sn^{4+} were employed. UV-Vis absorption spectra and photoluminescence excitation spectra were used to elucidate the band gap of Sn-doped ZnO QDs. Photoluminescence spectra were employed to study the change in the defects of Sn-doped ZnO QDs. Sn doping reduced the symmetry of the ZnO cell and stretched the cell. Furthermore, it also could change ZnO from a direct gap semiconductor to an indirect gap semiconductor. The experimental results and DFT calculations matched quite well. Both the DFT calculations and experimental results showed that with an increasing Sn content, the band gap of Sn-doped ZnO first decreased and then increased, whereas the band gap of the ZnO base only increased. Sn doping also changed the optical defects of the quantum dots from $V_O^{\cdot}$ defects to O_{Zn} and O_i defects.

Introduction

Zinc oxide (ZnO) is a wide band gap (3.37 eV) semiconductor with a large exciton binding energy (60 meV).[1,2] ZnO exhibited excellent UV-absorption and photoluminescence properties. Furthermore, ZnO is a non-toxic material and abundant in nature.

Colloidal quantum dots (QDs) have attracted much attention in recent years due to their amazing characteristics in optics. There are several ways to change the energy gap of QDs. The first way is to change their sizes by changing their synthetic methods. The energy gap of QDs enlarged when their sizes were reduced. The second way is to control the band structure of the bulk material by doping with other ions.

There has been much research on the use of ions to dope ZnO in recent years. As reported, the band gap of Al doped ZnSnO first decreased and then increased with more Al doping.[3] For Ni-doped ZnO, the value of the energy gap decreased as more Ni was added.[4] La was reported to increase the band gap of ZnO.[5]

However, for Sn-doped ZnO,[6] the results were different. Some researchers reported that Sn-doped ZnO had an increase

in the energy gap for both defect types at high Sn concentration.[7] In contrast, there are a few reports stating that the band gap of $Zn_{0.98−x}Mn_{0.02}Sn_xO$ decreased with increasing Sn content at low levels of Sn.[8] Moreover, there are still fewer studies on the difference between Sn^{2+} and Sn^{4+} doping on ZnO.

In this study, density functional theory (DFT) was used to investigate the crystal structure, band structure and band gap of Sn-doped ZnO. Both Sn^{2+} and Sn^{4+} were considered. To verify the DFT results, Sn^{2+}- and Sn^{4+}-doped ZnO QDs were synthesized *via* an ultrasonic method. UV-Vis absorption spectra and photoluminescence excitation spectra were used to characterize the band gap of Sn-doped ZnO QDs. Photoluminescence spectra were employed to study the change in the defects of Sn-doped ZnO QDs as well.

Experimental

Band structure calculation of $Zn_{1−x(y)}Sn_{x(y)}O$

The band structures of $Zn_{1−x(y)}Sn_{x(y)}O$ were calculated using CASTEP (8.0).[9] The geometric structure of each $Zn_{1−x(y)}Sn_{x(y)}O$ sample (x is for Sn^{2+}, y is for Sn^{4+}) was optimized using the Generalized Gradient Approximation (GGA) and Perdew–Burke–Ernzerhof (PBE)[10] with a cut-off energy of 340 eV. The Brillouin zone was sampled with $5 \times 5 \times 3$ Monkhorst and Pack k-points. The lattice parameters, as well as the atomic positions within the supercell, have been optimized until the forces and total energy converged within 0.015 eV Å^{-1} and 10^{-5} eV, respectively.

To make the crystal more symmetrical, we only added one Sn ion in a supercell. To create a $Zn_{1−x(y)}Sn_{x(y)}O$ compound with Sn concentrations of 12.5%, 6.25%, 4.17%, 2.78%, 1.85%, 1.39%

[a]College of Materials Science and Engineering, Nanjing Tech University, Nanjing 210009, China. E-mail: ngdzqt@163.com

[b]Jiangsu Collaborative Innovation Center for Advanced Inorganic Function Composites, Nanjing Tech University, Nanjing 210009, China

[c]School of Materials Science and Engineering, Georgia Institute of Technology, 771 Ferst Drive, Atlanta, GA 30332, USA

[d]Faculty of Engineering, The Chinese University of Hong Kong, Shatin 999077, Hong Kong, China

and 0%, with $2 \times 2 \times 1$, $2 \times 2 \times 2$, $3 \times 2 \times 2$, $3 \times 3 \times 2$, $3 \times 3 \times 3$, $4 \times 3 \times 3$ and $1 \times 1 \times 1$ unit cells were considered, respectively (Fig. 1).

Materials

Ethyl alcohol (99.7%), polyethylene glycol-400 (PEG-400, 99.0%), lithium hydroxide (LiOH·H$_2$O, 95.0%), oleic acid (OA, 99.0%), n-hexane (97.0%) were purchased from Shanghai Lingfeng Chemical Company. Zinc acetate (Zn(Ac)$_2$·2H$_2$O, 99.0%), stannic chloride (SnCl$_4$·5H$_2$O, 98.0%), stannous chloride (SnCl$_2$·2H$_2$O, 99.0%) were purchased from Xilong Chemical Company and used without further purification.

Synthesis of Zn$_{1-x(y)}$Sn$_{x(y)}$O QDs by ultrasonic method

As reported, an ultrasonic method has been a simple way to synthesize ZnO QDs with uniform sizes.[11,12] In this study, Sn-doped ZnO QDs samples were prepared via the ultrasonic method. To obtain 0.0025 mol Zn$_{1-x}$Sn$_x$O ($x = 0$, 0.01, 0.03, 0.05, 0.07, 0.09, Sn^{2+}) or Zn$_{1-y}$Sn$_y$O ($y = 0$, 0.01, 0.03, 0.05, 0.07, 0.09, Sn^{4+}) QDs, appropriate amounts (n(Zn) + n(Sn) = 0.0025 mol) of stannic chloride (SnCl$_4$·5H$_2$O) or stannous chloride (SnCl$_2$·2H$_2$O, 99.0%) and zinc acetate (Zn(Ac)$_2$) were dissolved in 100 mL of ethyl alcohol and kept in an ultrasonic dispersion for 30 min. Then, appropriate amounts of PEG-400 with n(PEG) : (n(Zn) + n(Sn)) = 1 : 1 were added[13] into the system with 40 min of ultrasonic dispersion. At the same time, 0.21 g (0.005 mol) LiOH was dissolved in 50 mL of ethyl alcohol and kept in an ultrasonic dispersion for 30 min. After that, the two solutions were mixed. Zn$_{1-x}$Sn$_x$O QDs were obtained after continuous ultrasonication (ultrasonic frequency = 53 kHz, ultrasonic power = 180 W) to promote the reaction at 40 °C for 30 min. Then, 0.6 mL of oleic acid (OA)[14,15] was used to precipitate the QDs. The white sediment was centrifuged for 5 min at 4000 rpm for 2–3 times and then washed with excess ethanol to remove any unreacted material. Finally, Zn$_{1-x}$Sn$_x$O QDs were dispersed in n-hexane for further use.

Measurement

The high resolution TEM (HRTEM) image of Sn doped ZnO nanostructure EDX and the selected area electron diffraction (SAED) were acquired on FEI Tecnai F30 TEM. The X-ray photoelectron spectroscopy (XPS) was collected on Thermo K-Alpha XPS. The photoluminescence spectra were obtained using a fluorescence spectrophotometer (Lumina, Thermo, U.S.A). For each sample, the emission spectrum was measured under the measured excitation peak as an excitation wavelength, and the excitation spectrum was measured under the measured emission peak as an emission wavelength.

The photoluminescence quantum yields (PL QYs) were calculated by the following equation, using Rhodamine 6G dissolved in water (QY = 95%) as reference:[16]

$$QY_{sample} = \left(\frac{F_{sample}}{F_{ref}} \right) \left(\frac{A_{ref}}{A_{sample}} \right) \left(\frac{n_{sample}^2}{n_{ref}^2} \right) QY_{ref} \quad (1)$$

where F is the measured fluorescence, A is the absorbance at the excitation wavelength, and n is the refractive index of the solvent.

The absorption spectra were recorded on a UV-Vis-NIR spectrophotometer (UV-3600, Shimadzu, Japan) using n-hexane as a reference.

The optical gap E_{gap} of ZnO QDs could be calculated by Formula (2):[17]

$$\alpha = \frac{A \left(h\nu - E_{gap} \right)^n}{h\nu} \quad (2)$$

where α is the absorption coefficient proportional to the absorbance, A is a constant and n is a constant equal to 1/2 for direct gap semiconductors and 2 for indirect gap semiconductors.[18]

Results and discussion

Sn^{2+} doped ZnO

The calculated cell parameters of Zn$_{1-x}$Sn$_x$O are shown in Table 1.

As shown in Table 1, with an increase in the Sn^{2+} content, the cell parameters changed. This implies that, with more Sn^{2+} doping, the space group of Zn$_{1-x}$Sn$_x$O first changed from hexagonal to monoclinic and then changed to triclinic. This means that the symmetry of Zn$_{1-x}$Sn$_x$O was reduced by Sn^{2+} doping. The cell volume of Zn$_{1-x}$Sn$_x$O was raised from 0.04759 nm^3 to 0.05194 nm^3 when x increased. This trend approached the reported experimental data.[19] Moreover, the length of the Sn–O bond increased from 0.2057 nm to 0.2242 nm. The reason for this was that size of Sn^{2+} ionic radii (0.112 nm) was much larger than that of the Zn^{2+} ion (0.074 nm). Sn^{2+} doping stretched the ZnO cells. For the Zn–O bond, the change in bond length was just from 0.1982 nm to 0.2032 nm, which then decreased to 0.2017 nm; thus the change was not significant.
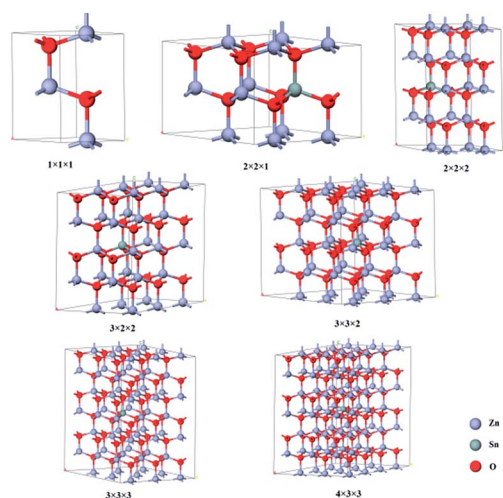

Fig. 1 The crystalline structure of Zn$_{1-x(y)}$Sn$_{x(y)}$O for x (y) = 0, 0.125, 0.0625, 0.0417, 0.0278, 0.0185 and 0.0139. Silver, dark green and dark red spheres are represented by Zn, Sn and O, respectively.

Table 1 Calculated cell parameters of $Zn_{1-x}Sn_xO$

Sn^{2+} content	a	b	c	α	β	γ	V	Sn–O	Zn–O
0%	0.3249 nm	0.3249 nm	0.5205 nm	90.0°	90.0°	120.0°	0.04759 nm³	—	0.1982 nm
1.39%	0.3249 nm	0.3249 nm	0.5205 nm	90.0°	90.0°	120.0°	0.04759 nm³	0.2057 nm	0.1981 nm
1.85%	0.3344 nm	0.3342 nm	0.5291 nm	90.0°	90.0°	121.0°	0.05067 nm³	0.2076 nm	0.2032 nm
2.78%	0.3329 nm	0.3322 nm	0.5374 nm	90.3°	90.1°	121.2°	0.05081 nm³	0.2066 nm	0.2026 nm
4.17%	0.3329 nm	0.3332 nm	0.5366 nm	90.1°	90.0°	120.9°	0.05107 nm³	0.2178 nm	0.2024 nm
6.25%	0.3348 nm	0.3348 nm	0.5380 nm	90.1°	89.9°	121.0°	0.05170 nm³	0.2202 nm	0.2026 nm
12.5%	0.3371 nm	0.3371 nm	0.5346 nm	90.2°	89.9°	121.3°	0.05194 nm³	0.2242 nm	0.2017 nm

This increment was due to the cell enlarging, and the decrement was due to the Sn–O bond stretching.

The calculated band structure of $Zn_{1-x}Sn_xO$ is shown in Fig. 2. It suggests that $Zn_{1-x}Sn_xO$ changed from direct gap semiconductors to indirect gap semiconductors with the Sn^{2+} content increasing to $x = 0.0278$. The E_{gap} of $Zn_{1-x}Sn_xO$ first decreased from 0.806 eV to 0.197 eV when the Sn^{2+} content increased from 0 to 0.0625 and then it increased to 0.722 eV with increasing Sn^{2+} content.

As reported, the band gap of ZnO should be 3.37 eV. However, our calculated results showed that the band gap of ZnO was 0.806 eV, which is much less than the reported band gap. The reason for this was that there are some deficiencies of the DFT/GGA during the calculations of transition metal oxides, particularly for ZnO.[20–22] Usually, the LDA+U method was employed to solve this problem. However, the LDA+U method does not lead to the correction of the band gap.[22,23] The main idea for this study was to discuss the effect of Sn content on the band structure of Sn-doped ZnO. As a result, only the changing trend in the band structure was required, the exact band structure, especially the exact band gap was not required. In other words, LDA+U was not required in this study.[4,7]

Fig. S1† shows the calculated total DOS (DOS) and partial DOS (PDOS) of $Zn_{1-x}Sn_xO$. As shown in this figure, the valence band maximum was mainly derived from the O 2p orbital, and the conduction band minimum was mainly derived from Sn 5s and Sn 5p states.[23] It appeared that with more Sn^{2+} doping, the shape, location and energy of these PDOS peaks changed. Sn 5p states became stronger, whereas O 2p orbital became weaker.

Fig. 3 shows the HRTEM and EDX figures of Sn^{2+} doped $Zn_{0.95}Sn_{0.05}O$ and $Zn_{0.91}Sn_{0.09}O$ QDs synthesized at 40 °C with 180 W of ultrasonic power for 30 min. It was observed that Sn^{2+} doped ZnO QDs have a uniform size around 2.6 nm, which was similar to the ZnO QDs synthesized under the same conditions.[14] It also means that size effects on the band gap of Sn^{2+}-doped ZnO QDs could be ignored.

Moreover, it was difficult to find the SnO_2 (0.335) or SnO (0.299) phase[24–26] in the HRTEM figure. It appeared that Sn^{2+}-
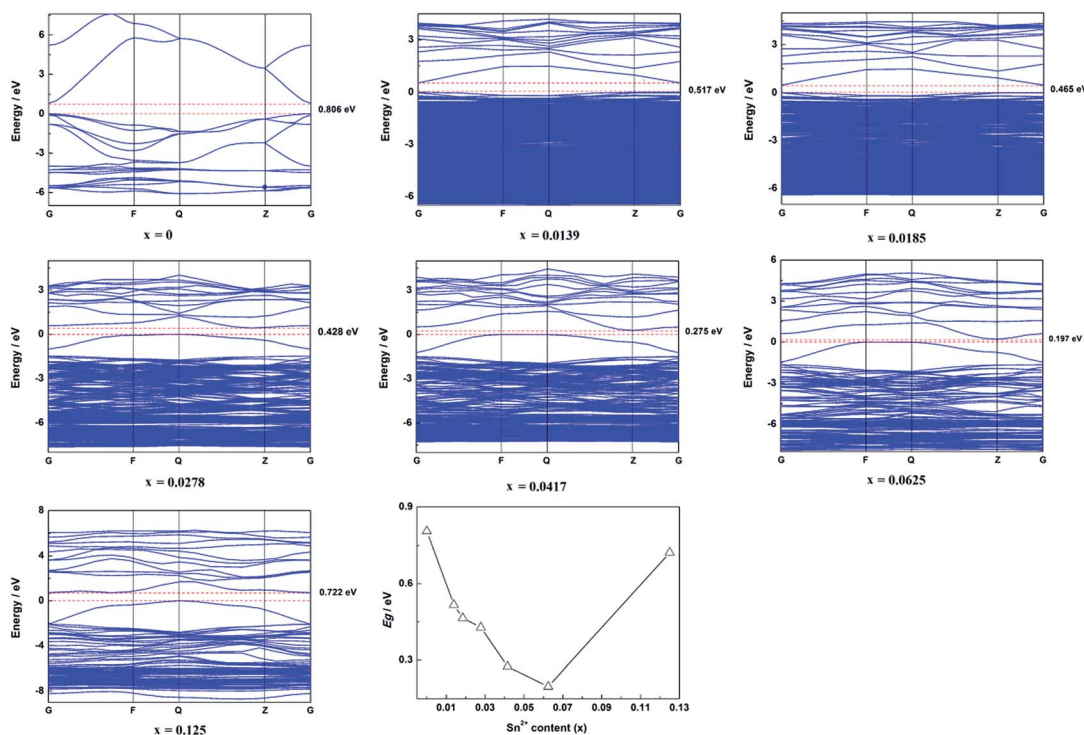

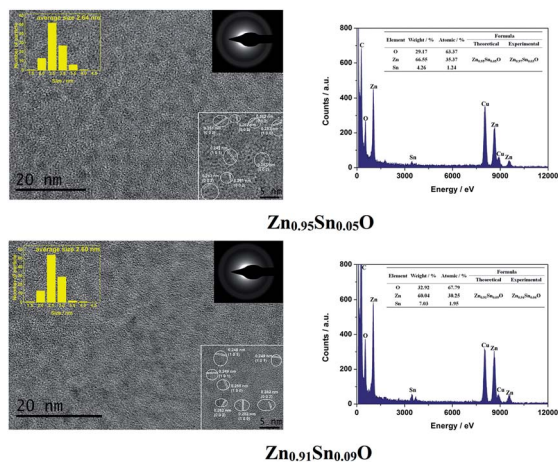**Fig. 2** Calculated band structure and summarized E_{gap} of $Zn_{1-x}Sn_xO$.

Fig. 3 HRTEM and EDX of Sn^{2+} doped $Zn_{0.95}Sn_{0.05}O$ and $Zn_{0.91}Sn_{0.09}O$ QDs synthesized at 40 °C with 180 W of ultrasonic power for 30 min.

doped ZnO QDs still maintained the main phase of ZnO, which was different from those of the Sn-doped ZnO NPs with a high Sn concentration[24–26] but was the same as that of the Sb doped ZnO with a low Sb concentration.[27] The interplanar spacing increased with increasing Sn^{2+} concentration. This was similar to the trend in the calculated cell parameters of $Zn_{1-x}Sn_xO$, as shown in Table 1.

Both Zn and Sn appeared in the EDX spectra. The atomic percentage of Zn, Sn and O are given in the figure as well. The possible formulas of these samples were $Zn_{0.97}Sn_{0.03}O$ and $Zn_{0.94}Sn_{0.06}O$, which approached to the theoretical formulas $Zn_{0.95}Sn_{0.05}O$ and $Zn_{0.91}Sn_{0.09}O$. Therefore, Sn was successfully doped into the lattice of ZnO.

Fig. 4 shows the XPS spectra of $Zn_{1-x}Sn_xO$ QDs synthesized at 40 °C with 180 W of ultrasonic power for 30 min. All the data

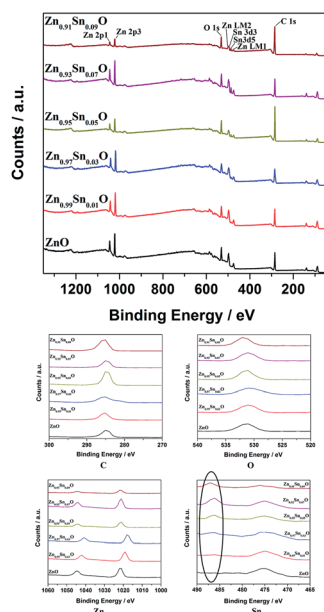**Fig. 4** XPS spectra of $Zn_{1-x}Sn_xO$ QDs synthesized at 40 °C with 180 W of ultrasonic power for 30 min.

were corrected with respect to the standard peak of C 1s at 284.6 eV.[27–30] As shown in Fig. 4, for all the samples, both Sn and Zn peaks could be found in the XPS spectra. This was the same as the results from the EDX spectra. All the peaks of O, Zn and Sn were narrow and symmetric with FWHMs about 3 eV.

For Zn 2p1 and Zn 2p3 at the same x values, the binding energy first decreased when x increased to 3 and then returned to the ZnO level.

The binding energy of O 1s peaks centered at 530.15 eV (O I) belongs to the O^{2-} ions in the wurtzite structure of ZnO. Peaks centered at 531.25 eV (O II) belong to the oxygen vacancy defects, and peaks centered at 532.40 eV (O III) belong to the loosely bound oxygen on the surface of ZnO.[30] Fitted spectra of O 1s peaks of Sn^{2+}-doped ZnO are shown in Fig. S2.† It shows that, when the x value was less than 3, the main charge state of oxygen was the O^{2-} ions in the wurtzite structure of ZnO. Then, the main oxygen state changed to oxygen vacancy defects and finally, to loosely bound oxygen.

The reason for the decrease in binding energy when x was less than 3 could be that when the concentration of Sn^{2+} was low, the way of Sn doping was interstitial. For a high Sn^{2+} concentration, the way of Sn doping changed to substitution. When x was larger than 5, with more Sn^{2+} doping, the concentration of $V_O^{\cdot}$ defects decreased, whereas the concentration of O_{Zn} and O_i defects increased.

The intensity of Sn 3d5 and Sn 3d3 increased with increasing x values. This means that the real Sn concentration in Sn doped ZnO QDs increased with more Sn^{2+} doping. The atomic percentages of Zn and Sn for all the samples are shown in Table 2. It appears that, with increases in the Sn^{2+} concentration in the raw material, the Sn concentration in $Zn_{1-x}Sn_xO$ QDs increased. Even the value of the Sn content obtained from XPS was much larger than the theoretical Sn concentration. The changing trend in the Sn concentration still was close to what we expected.

Fig. 5(a) shows the UV-Vis absorption spectra of $Zn_{1-x}Sn_xO$ QDs synthesized at 40 °C with 180 W of ultrasonic power for 30 min. All sample absorptions started from about 350 nm. As the Sn^{2+} content increased, the 99% absorption wavelength first increased from 350.5 nm to 370.5 nm until $x = 0.03$ and then decreased to 343 nm.

ZnO is a direct gap semiconductor,[31,32] which can be seen in Fig. 2. Formula (2) could change to Formula (3). This also means that $(\alpha h\nu)^2$ is proportional to $(h\nu - E_{gap})$, and E_{gap} is the intercept on the x-axis.

Table 2 Atomic percentage of Zn and Sn and possible formulas. of $Zn_{1-x}Sn_xO$

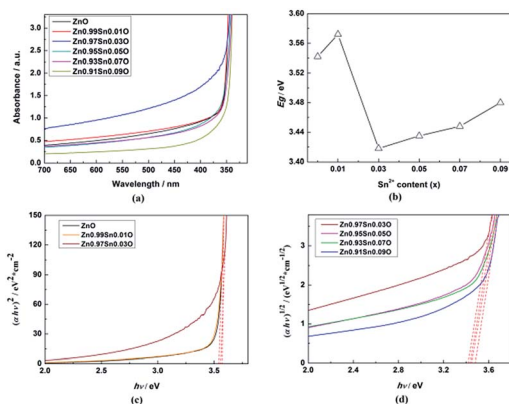| x value	Zn/at%	Sn/at%	Formula
0	100	0	ZnO
1	99.5	0.5	$Zn_{0.995}Sn_{0.005}O$
3	98	2	$Zn_{0.98}Sn_{0.02}O$
5	93	7	$Zn_{0.93}Sn_{0.07}O$
7	88	12	$Zn_{0.88}Sn_{0.12}O$
9	83	17	$Zn_{0.83}Sn_{0.17}O$

Fig. 5 (a) UV-Vis absorption spectra, (b) calculated E_{gap}, (c) the plot of $(\alpha h\nu)^2$ *vs.* $(h\nu)$, (d) the plot of $(\alpha h\nu)^{1/2}$ *vs.* $(h\nu)$ of $Zn_{1-x}Sn_xO$ QDs synthesized at 40 °C with 180 W of ultrasonic power for 30 min.

$$(\alpha h\nu)^2 = A^2(h\nu - E_{gap}) \tag{3}$$

As shown in Fig. 5, the calculated E_{gap} for ZnO QDs is 3.542 eV, which is similar to the reported band gap of ZnO.

After Sn^{2+} doping, $Zn_{1-x}Sn_xO$ QDs changed to an indirect gap semiconductor, as shown in Fig. 2. Formula (2) could also change to Formula (4), which means that $(\alpha h\nu)^{1/2}$ is proportional to $(h\nu - E_{gap})$, and E_{gap} is the intercept on the x-axis.

$$(\alpha h\nu)^{1/2} = A(h\nu - E_{gap}) \tag{4}$$

The calculated E_{gap} for all samples is given in Fig. 5(b–d). As shown in Fig. 5(b), with increasing Sn^{2+} content, the E_{gap} of $Zn_{1-x}Sn_xO$ QDs first increased from 3.542 eV to 3.572 eV, dropped to 3.418 eV, and finally increased to 3.480 eV. E_{gap} increased to the minimum point when the Sn^{2+} content reached 0.03. All of these are larger than the band gap of a ZnO single-crystal (3.37 eV).[31,32] This was due to the energy band of QDs being quasi-continuous owing to their small size.[31]

The calculated E_{gap} of $Zn_{1-x}Sn_xO$ first decreased then increased, and the inflection point of Sn^{2+} content (x) is 0.03, which is shown in Fig. 2. It seem that, changing trends in the calculated and experimental E_{gap} of $Zn_{1-x}Sn_xO$ are almost the same.

Photoluminescence properties could reflect the band structures, sizes and defects of $Zn_{1-x}Sn_xO$ QDs. Fig. 6 shows the photoluminescence properties of $Zn_{1-x}Sn_xO$ QDs synthesized at 40 °C with 180 W of ultrasonic power for 30 min.

As reported, the energy bands of quantum dots are determined by the size and band structures of $Zn_{1-x}Sn_xO$ QDs. Under same quantum dot concentration,[15,18] the change in $Zn_{1-x}Sn_xO$ QDs excitation peaks was connected to the change in $Zn_{1-x}Sn_xO$ QDs band structures and sizes.[13] For the ZnO quantum dots synthesized under the same condition, the size could be almost the same, meaning the excitation peaks could reflect the band structures of $Zn_{1-x}Sn_xO$ QDs.

Fig. 6(b) shows the excitation spectrum of the $Zn_{1-x}Sn_xO$ QDs. As shown in Fig. 6(b) and (c), with increasing Sn^{2+} content, the excitation peaks of $Zn_{1-x}Sn_xO$ QDs first decreased from 357 nm to 339 nm and then remained unchanged. The
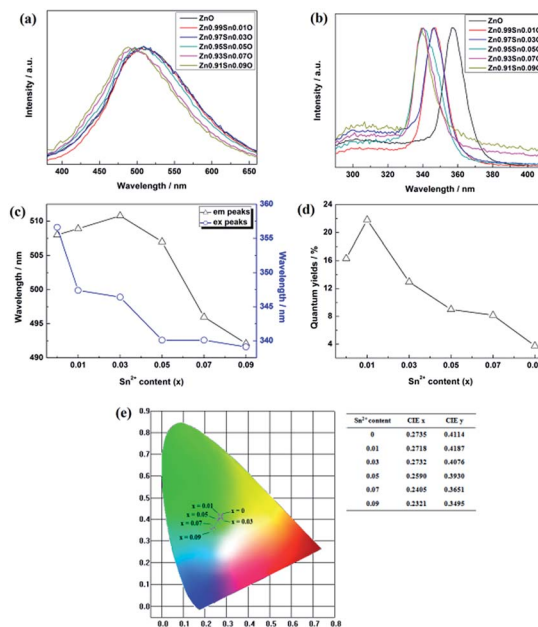

Fig. 6 Photoluminescence properties of $Zn_{1-x}Sn_xO$ QDs synthesized at 40 °C with 180 W of ultrasonic power for 30 min. (a) emission spectra (b) excitation spectra (c) emission and excitation peaks (d) quantum yield (e) CIE diagram.

excitation peak of $Zn_{1-x}Sn_xO$ QDs is related to the energy band of ZnO base.[5,33] This means that as the Sn^{2+} content increased, the energy band of the ZnO base increased.

Compared to the changing trend of E_{gap} obtained by the absorption spectrum in Fig. 5, the trend is different. The E_{gap}, calculated from the absorption spectrum, first decreased, then increased with more Sn^{2+} doping, and then approached the calculated results. However, the band gap inferred from the excitation peaks increased along with the Sn^{2+} content increasing. Due to the Moss–Burstein effect,[34] when doping Sn atoms into the bulk, the band gap of ZnO grew wider, resulting in a blue shift of the excitation peaks.

To verify this, Dmol[3] was employed to calculate the orbital properties of Sn^{2+}-doped ZnO.[35,36] As shown in Fig. S3,† with an increasing Sn^{2+} content, the conduct band minimum (CBM) first decreased and then increased, while the valence band maximum (VBM) decreased. Moreover, $E_v - E_c$ increased with Sn^{2+} doping. This result approached the changing trend in the excitation peaks.

Fig. 6(a) and (e) show the emission spectra of $Zn_{1-x}Sn_xO$ QDs. Spectral shapes of $Zn_{1-x}Sn_xO$ QDs synthesized with different Sn^{2+} content were almost the same. The emission peaks were between 490 nm to 510 nm. With the addition of Sn^{2+}, the emission peaks and blue emission shifted from yellow-green to blue-green.

The trend in emission and excitation peaks reflected the transformation between optical defects inside $Zn_{1-x}Sn_xO$ QDs. As reported, the green photoluminescence near 500 nm of ZnO bulk (with the optical gap of 3.37 eV) is mainly brought about by (1) a transition from near the conduction band edge to a deep acceptor level by O_{Zn} (2.38 eV) or O_i (2.24 eV), and (2) the transition from a deep donor level by $V_o^{\cdot}$ to a valence band (2.43

eV).[5,11,37–39] This implies that, for the ZnO QDs with O_{Zn} or O_i defects, the changing trend in emission peaks should be the same as that of the excitation peaks. While for ZnO QDs with $V_o^{\cdot}$ defects, the emission peaks might stay at about 510 nm, regardless of the change in size of the ZnO QDs.

Fig. 6(c) shows that with increasing Sn^{2+} content, the emission peaks first increased from 508 nm to 511 nm, and then dropped to about 492 nm again. It means that, under low Sn^{2+} content, main optical defects of $Zn_{1-x}Sn_xO$ QDs were $V_o^{\cdot}$ defects. With increasing Sn^{2+} content, some $V_o^{\cdot}$ defects changed to O_{Zn} and O_i defects. This is due to the fact that the Sn^{2+} was not stable and could easily change to Sn^{4+}. This process introduced O into $Zn_{1-x}Sn_xO$ QDs, which eliminated the $V_o^{\cdot}$ defects and created O_{Zn} and O_i defects.

Fig. 6(d) shows the trend in $Zn_{1-x}Sn_xO$ QDs quantum yields influenced by Sn^{2+} content. The quantum yields of $Zn_{1-x}Sn_xO$ QDs first increased from 16.3% to 21.8% with little Sn^{2+} doping when $x = 0.01$. Then, the quantum yield sharply decreased to 3.7% with more Sn^{2+} doping.

It was reported that quantum yields of ZnO QDs are related to their optical defects. Introducing more optical defects[15] could improve the quantum yields of ZnO QDs. However, quantum yields of QDs were also determined by the electronic traps,[40] particularly the dangling bond defects on the surface of ZnO QDs. This means that passivation of the surface-state traps would improve the quantum yields of QDs as well.[41] With an increase in Sn^{2+} content, the OH^- dangling bonds on the surface of $Zn_{1-x}Sn_xO$ QDs decreased due to the Sn^{2+}–Sn^{4+} transformation. This is advantageous to increase the quantum yield. However, with more Sn^{2+} doping, the Sn^{2+}–Sn^{4+} transformation caused the concentration of $V_o^{\cdot}$ defects to decrease. This was the reason for the decrement of quantum yields of $Zn_{1-x}Sn_xO$ QDs when there were more Sn^{2+} ions. Moreover, it was reported that an indirect gap semiconductor has a poorer photoluminescence than that for the direct gap semiconductor.[42] As mentioned, with Sn^{2+} content (x) increased to 0.03, the $Zn_{1-x}Sn_xO$ QDs changed from direct gap semiconductors to indirect gap semiconductors. As a result, the quantum yields slightly increased at first and then sharply dropped.

Sn^{4+} doped ZnO

The calculated cell parameters of $Zn_{1-y}Sn_yO$ are shown in Table 3.

As shown in Table 3, with an increase in the Sn^{4+} content, the cell parameters changed. Similar to that of $Zn_{1-x}Sn_xO$, the symmetry of $Zn_{1-y}Sn_yO$ was reduced by Sn^{4+} doping. With more Sn^{4+} doping, the space group of $Zn_{1-y}Sn_yO$ first changed from hexagonal to monoclinic and then changed to triclinic. The cell volume of $Zn_{1-y}Sn_yO$ increased from 0.04759 nm^3 to 0.05206 nm^3 when y increased. The length of the Sn–O bond increased from 0.2058 nm to 0.2242 nm. Even the sizes of Sn^{4+} ionic radii (0.069 nm) were smaller than that of the Zn^{2+} ion (0.074 nm). The charge of Sn^{4+} is larger than that of Zn^{2+}, which means that the repulsion between Sn^{4+} and Zn^{2+} is larger than that between Zn^{2+} and Zn^{2+} as well as that between Sn^{2+} and Zn^{2+}. That is why Sn^{4+} doping could also stretch the ZnO cells. However, for the Zn–O bond, the change in bond length was just from 0.1982 nm to 0.2026 nm, and then it decreased to 0.2018 nm, which was not significant. The increment was because of the cell enlarging, and the decrement was because of the Sn–O bond stretching.

The calculated band structure of $Zn_{1-y}Sn_yO$ is shown in Fig. 7. It suggests that $Zn_{1-y}Sn_yO$ changed from a direct gap semiconductor to an indirect gap semiconductor with an increase in the Sn^{4+} content to $y = 0.0185$, which is similar to that of Sn^{2+} doping ZnO. The E_{gap} of $Zn_{1-y}Sn_yO$ first decreased from 0.806 eV to 0.224 eV when the Sn^{4+} content rose from 0 to 0.0278 and then it increased to 0.701 eV with a rise in the Sn^{4+} content.

Compared to the calculated E_{gap} of Sn^{2+}-doped ZnO ($Zn_{1-x}Sn_xO$), there are some differences. First, the inflection point of the E_{gap} is different. For $Zn_{1-x}Sn_xO$, the inflection point is about $x = 0.0625$, whereas for $Zn_{1-y}Sn_yO$, $y = 0.0278$. Second, the value of E_{gap} for the inflection point is different. For $Zn_{1-y}Sn_yO$, it is 0.224 eV, whereas for $Zn_{1-x}Sn_xO$, it is 0.197 eV, which is smaller than that of $Zn_{1-y}Sn_yO$.

Fig. S4† displays the calculated total DOS (DOS) and partial DOS (PDOS) of $Zn_{1-y}Sn_yO$. The changing trend in total DOS (DOS) and partial DOS (PDOS) of $Zn_{1-y}Sn_yO$ is similar to those of $Zn_{1-x}Sn_xO$. As shown in the figure, the valence band maximum is also derived mainly from the O 2p orbital, and the conduction band minimum is derived mainly from Sn 5s and Sn 5p states.[23] It appears that, with more Sn^{4+} doping, the shape, location and energy of these PDOS peaks changed. Sn 5p states became stronger, whereas the O 2p orbital became weaker. Moreover, compared with the Sn^{2+}-doped ZnO samples, the shape, location and energy of Sn 5p states were quite different. That might be the reason why the trend in the band gap was different.

Table 3 Calculated cell parameters of $Zn_{1-y}Sn_yO$

Sn^{4+} content	a	b	c	α	β	γ	V	Sn–O	Zn–O
0%	0.3249 nm	0.3249 nm	0.5205 nm	90.0°	90.0°	120.0°	0.04759 nm^3	—	0.1982 nm
1.39%	0.3249 nm	0.3249 nm	0.5205 nm	90.0°	90.0°	120.0°	0.04759 nm^3	0.2058 nm	0.1981 nm
1.85%	0.3273 nm	0.3273 nm	0.5238 nm	90.0°	90.0°	120.1°	0.04855 nm^3	0.2112 nm	0.1997 nm
2.78%	0.3322 nm	0.3321 nm	0.5385 nm	90.0°	90.0°	120.7°	0.05103 nm^3	0.2084 nm	0.2026 nm
4.17%	0.3331 nm	0.3338 nm	0.5363 nm	90.0°	90.0°	121.0°	0.05113 nm^3	0.2176 nm	0.2025 nm
6.25%	0.3349 nm	0.3348 nm	0.5382 nm	90.2°	89.9°	121.0°	0.05173 nm^3	0.2202 nm	0.2026 nm
12.5%	0.3377 nm	0.3376 nm	0.5341 nm	90.4°	89.6°	121.2°	0.05206 nm^3	0.2242 nm	0.2018 nm

Fig. 8 shows the HRTEM and EDX figures of Sn^{4+} doped $Zn_{0.95}Sn_{0.05}O$ and $Zn_{0.91}Sn_{0.09}O$ QDs synthesized at 40 °C with 180 W of ultrasonic power for 30 min. Moreover, Sn^{4+} doped ZnO QDs have a uniform size around 2.6 nm, which is similar to that of the ZnO QDs[14] and Sn^{2+}-doped ZnO QDs synthesized under the same conditions. Sizes effects on the band gap of Sn^{4+} doped ZnO QDs could also be ignored.

It is difficult to find a SnO_2 (0.335) or SnO (0.299) phase[24–26] in the figure as well. It appears that Sn^{4+} doped ZnO QDs also could maintain the main phase of ZnO, which is similar to Sn^{2+} doped ZnO with a low Sn concentration. The interplanar spacing increased with increasing Sn^{4+} concentration. Interplanar spacings of $Zn_{1-y}Sn_yO$ were larger than those of $Zn_{1-x}Sn_xO$ at the same Sn concentration. This approached the calculated results of $Zn_{1-y}Sn_yO$ shown in Table 3.

Both Zn and Sn could be found in the EDX spectra as well. The atomic percentages of Zn, Sn and O are given in the figure as well. The possible formulas of these samples were $Zn_{0.97}Sn_{0.03}O$ and $Zn_{0.91}Sn_{0.09}O$, which also approached the theoretical formulas $Zn_{0.95}Sn_{0.05}O$ and $Zn_{0.91}Sn_{0.09}O$. Therefore, Sn^{4+} was successfully doped into the lattice of ZnO just like Sn^{2+} ions.

Fig. 9 shows the XPS spectra of $Zn_{1-y}Sn_yO$ QDs synthesized at 40 °C with 180 W of ultrasonic power for 30 min. All the data were corrected with respect to the standard peak of C 1s at 284.6 eV. As shown in Fig. 9, for all the samples, both Sn and Zn peaks are observed in the XPS spectra. The peaks of O, Zn and Sn were narrow and symmetrical with FWHM about 3 eV. This is same as the results of EDX shown in Fig. 8.

In the same way as Sn^{2+}-doped ZnO QDs, the binding energy of Zn 2p1 and Zn 2p3 peaks first decreased when y increased to 3 and then returned to the ZnO level.

It appears that the changing trend in the type of oxygen was almost the same as that of the Sn^{2+} doped ZnO QDs. When the y value was less than 3, the main type of oxygen was the O^{2-} ions in the wurtzite structure of ZnO. This could be due to the same reason as that in Sn^{2+} doped ZnO QDs, mentioned earlier.

However, there are fewer $V_o^{·}$ defects in Sn^{4+}-doped ZnO QDs than in Sn^{2+}-doped ZnO QDs. The reason for this is that, in Sn^{4+}-
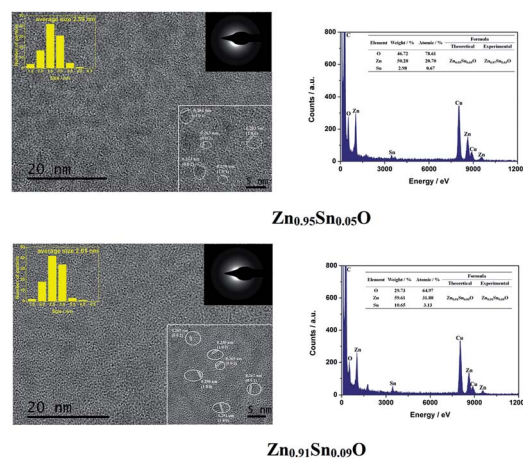

Fig. 8 HRTEM and EDX of Sn^{4+} doped $Zn_{0.95}Sn_{0.05}O$ and $Zn_{0.91}Sn_{0.09}O$ QDs synthesized at 40 °C with 180 W of ultrasonic power for 30 min.
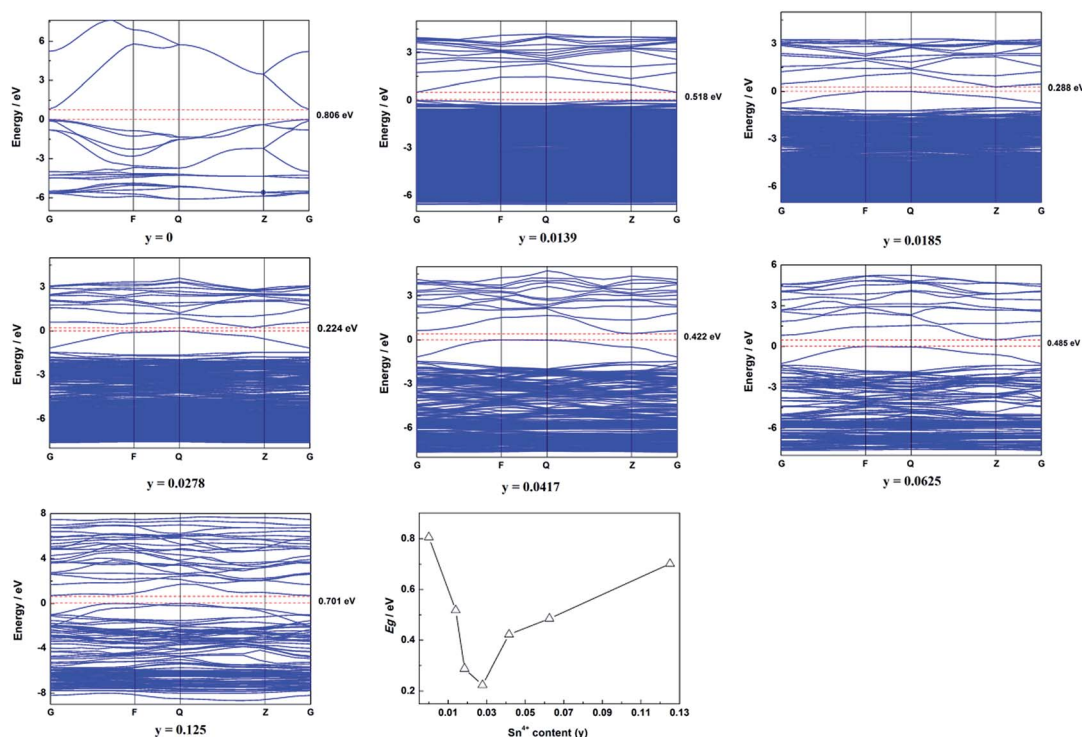

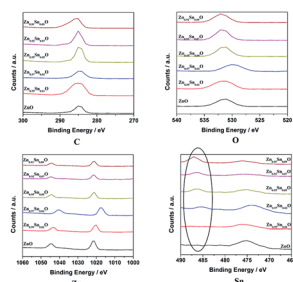Fig. 7 Calculated band structure and summarized E_{gap} of $Zn_{1-y}Sn_yO$.

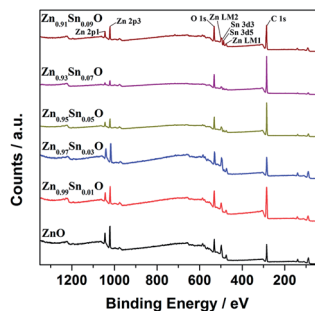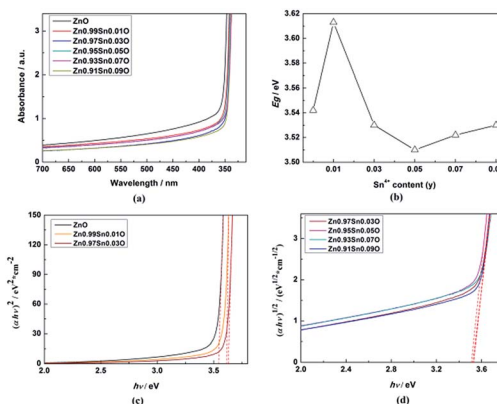Fig. 9 XPS spectra of $Zn_{1-y}Sn_yO$ QDs synthesized at 40 °C with 180 W of ultrasonic power for 30 min.

Fig. 10 (a) UV-Vis absorption spectra, (b) calculated E_{gap}, (c) the plot of $(\alpha h\nu)^2$ vs. $(h\nu)$, (d) the plot of $(\alpha h\nu)^{1/2}$ vs. $(h\nu)$ of $Zn_{1-y}Sn_yO$ QDs synthesized at 40 °C with 180 W of ultrasonic power for 30 min.

doped ZnO QDs, Sn^{4+} has a larger charge than Zn^{2+}, and $V_o^{\cdot}$ defects could not exist stably.

The reason could also be that when the concentration of Sn^{4+} is low, the way of Sn doping is interstitial. However, for high Sn^{4+} concentration, the way of Sn doping changed to substitution, which is similar to that of Sn^{2+}-doped ZnO QDs.

The intensity of Sn 3d5 and Sn 3d3 increased with increasing y values as well. This suggests that the Sn concentration in Sn-doped ZnO QDs increased with more Sn^{4+} doping. The atomic percentage of Zn and Sn for all of the samples is shown in Table 4. It appears that with an increasing Sn^{4+} concentration in the raw material, the Sn concentration in $Zn_{1-y}Sn_yO$ QDs increased. The changing trend in the Sn concentration still approached the expected trend.

Fig. 10(a) displays the UV-Vis absorption spectra of $Zn_{1-y}Sn_yO$ QDs synthesized at 40 °C with 180 W of ultrasonic power for 30 min. All sample absorptions started from about 350 nm. With an increasing Sn^{4+} content, the 99% absorption wavelength decreased from 350.5 nm to 341 nm when $y = 0.03$ and then remained at the same level.

As shown in Fig. 7, when the content of Sn^{4+} was raised to $y = 0.0278$, $Zn_{1-y}Sn_yO$ changed from a direct gap semiconductor to an indirect gap semiconductor. Formula (3) and (4) could also be used to calculate the E_{gap} of $Zn_{1-y}Sn_yO$ QDs.

The calculated E_{gap} for all samples is given in Fig. 10(b–d). As shown in Fig. 10(b), with increasing Sn^{4+} content, the E_{gap} of $Zn_{1-y}Sn_yO$ QDs first increased from 3.542 eV to 3.613 eV and then dropped to 3.510 eV, but finally rose to 3.530 eV. The E_{gap} reached the minimum point when the Sn^{4+} content reached 0.05.

The calculated E_{gap} of $Zn_{1-y}Sn_yO$ first decreased and then increased, and the inflection point of Sn^{4+} content (y) was
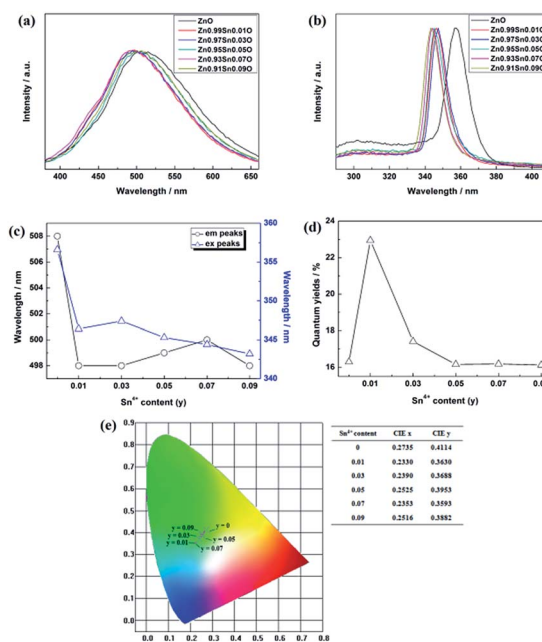

Fig. 11 Photoluminescence properties of $Zn_{1-y}Sn_yO$ QDs synthesized at 40 °C with 180 W of ultrasonic power for 30 min. (a) emission spectra (b) excitation spectra (c) emission and excitation peaks (d) quantum yield (e) CIE diagram.

Table 4 Atomic percentage of Zn and Sn and possible formulas of $Zn_{1-y}Sn_yO$

x value	Zn/at%	Sn/at%	Formula
0	100	0	ZnO
1	99.6	0.4	$Zn_{0.996}Sn_{0.004}O$
3	94	6	$Zn_{0.94}Sn_{0.06}O$
5	91	9	$Zn_{0.91}Sn_{0.09}O$
7	86	14	$Zn_{0.86}Sn_{0.14}O$
9	81	19	$Zn_{0.81}Sn_{0.19}O$

0.0278 (Fig. 7). The changing trend in the calculated E_{gap} of $Zn_{1-y}Sn_yO$ was identical to that of the experimental E_{gap}.

Compared to Sn^{2+}-doped samples, the E_{gap} of all $Zn_{1-y}Sn_yO$ samples was larger than those of $Zn_{1-x}Sn_xO$ samples. This phenomenon corresponds to the calculated results. It implies that the impurity levels of Sn^{4+} are higher than those of Sn^{2+}.

Fig. 11 shows the photoluminescence properties of Zn_{1-y}-Sn_yO QDs synthesized at 40 °C with 180 W of ultrasonic power for 30 min.

Fig. 11(b) shows the excitation spectrum of the $Zn_{1-y}Sn_yO$ QDs. The excitation peak of Sn-doped ZnO QDs is related to the energy band of the ZnO base. From Fig. 11(b) and (c), it is clearly seen that with increasing Sn^{4+} content, the excitation peaks of $Zn_{1-y}Sn_yO$ QDs decreased from 357 nm to 343 nm. This suggests that the energy band of the ZnO base increased with an increasing Sn^{4+} content as well.

Compared to the results obtained by the absorption spectrum in Fig. 10, the changing trend is different. For the E_{gap} calculated from the absorption spectrum, it first decreased and then increased with Sn^{4+} doping. However, the E_{gap} inferred from the excitation peaks increased along with an increasing Sn^{4+} content. This trend is the same as that of the Sn^{2+}-doped samples for the same reason mentioned in Section 3.1. Furthermore, the excitation peaks of $Zn_{1-y}Sn_yO$ QDs were larger than those of $Zn_{1-x}Sn_xO$ QDs for same Sn content. This means that the band gaps of Sn^{2+}-doped ZnO bases were larger than those of Sn^{4+}-doped ZnO bases. However, the opposite of this was observed for the E_{gap} of $Zn_{1-y}Sn_yO$ QDs and $Zn_{1-x}Sn_xO$ QDs. This means that Sn^{2+} could enlarge the band gap of the ZnO base more effectively than Sn^{4+}, while the energy levels of Sn^{4+} were higher than those of Sn^{2+}.

To verify this, Dmol³ was also employed to calculate the orbital properties of Sn^{4+}-doped ZnO.[35,36] As shown in Fig. S6,† with an increasing Sn^{4+} content, the CBM first decreased and then increased, while the VBM decreased, and $E_v - E_c$ increased with Sn^{4+} doping. Compared to Sn^{2+} doped ZnO, the changing trends in both CBM, VBM and $E_v - E_c$ are almost the same. Furthermore, $E_v - E_c$ of Sn^{2+}-doped ZnO was larger than that of Sn^{4+}-doped ZnO. Moreover, these results approached the results obtained by the excitation peaks.

Fig. 11(a) and (e) show the emission spectra of $Zn_{1-y}Sn_yO$ QDs. The spectral shapes of $Zn_{1-y}Sn_yO$ QDs synthesized with different Sn^{4+} content are almost the same. The emission peaks were between 490 nm to 510 nm. With the addition of Sn^{4+}, the emission peaks and emitting color first blue-shifted from yellow-green to blue-green and then redshifted to green again.

Fig. 11(c) shows that with an increasing Sn^{4+} content, the emission peaks decreased from 508 nm to 498 nm and then remained at the same level. This implies that for Sn^{4+}-doped ZnO QDs, the main optical defects were O_i and O_{Zn} defects. The reason for this is that the valence of Sn^{4+} is 4, which is larger than Zn^{2+} and Sn^{2+}. To maintain the conservation of electricity, $V_o^{\cdot}$ defects could not exist stably in the $Zn_{1-y}Sn_yO$ crystal, while O_i and O_{Zn} defects could exist.

Fig. 11(d) shows the changing trend of $Zn_{1-y}Sn_yO$ QDs quantum yields influenced by the Sn^{4+} content. The quantum yields of $Zn_{1-x}Sn_xO$ QDs first increased from 16.3% to 22.9%

with a slight amount of Sn^{4+} doping when $y = 0.01$. Then, the quantum yield decreased to 16.2% when the Sn^{4+} content increased to 0.05, and finally remained at the same level. There is no doubt that quantum yields of $Zn_{1-y}Sn_yO$ QDs were larger than those of $Zn_{1-x}Sn_xO$ QDs. With an increased Sn^{4+} content, the concentration of O_i and O_{Zn} defects increased. Moreover, OH^- dangling bonds on the surface of $Zn_{1-y}Sn_yO$ QDs decreased due to the formation of O_i and O_{Zn} defects as well. These are advantageous to increase the quantum yield.

For the negative part of quantum yield, after the Sn^{4+} content (y) increased to 0.03, $Zn_{1-y}Sn_yO$ QDs changed from a direct gap semiconductor to an indirect gap semiconductor. As mentioned, the indirect gap could reduce the luminescence. As a result, the quantum yields decreased when the Sn^{4+} content reached 0.03. However, more Sn^{4+} doping means more O_i and O_{Zn} optical defects and less OH^- dangling bonds on the surface. The positive part and negative part of $Zn_{1-y}Sn_yO$ QDs quantum yields could counteract. This is why the quantum yields of $Zn_{1-y}Sn_yO$ QDs remained at the same level when the Sn^{4+} content was larger than 0.05.

Compared to that of $Zn_{1-x}Sn_xO$ QDs, the changing trend of optical defects concentration in $Zn_{1-y}Sn_yO$ QDs is different. As mentioned in Section 3.1 for the $Zn_{1-x}Sn_xO$ QDs, with an increasing Sn^{2+} content, the concentration of their optical defects $V_o^{\cdot}$ decreased because of the creation of O_i and O_{Zn} defects. However, the main optical defects in $Zn_{1-y}Sn_yO$ QDs were O_i and O_{Zn} defects. With an increasing Sn^{4+} content, the concentration of optical defects increased. This is a possible reason why the quantum yields of $Zn_{1-y}Sn_yO$ QDs were larger than those of $Zn_{1-x}Sn_xO$ QDs.

Conclusions

In conclusion, the structure and band structure of Sn-doped ZnO QDs were investigated *via* DFT calculations and optical properties. It appears that both Sn^{2+} and Sn^{4+} doping could change ZnO from direct gap semiconductors to indirect gap semiconductors. With an increased Sn content, the band gap of Sn-doped ZnO first decreased and then increased. Sn^{2+} doping could reduce the band gap further. For the Sn-doped ZnO QDs synthesized by an ultrasonic method, the trends in the band gap were almost same as those obtained by DFT calculations. The band gap first decreased then increased with more Sn doping. Sn^{4+}-doped ZnO QDs had a larger band gap than that of Sn^{2+}-doped ZnO QDs.

The changing trend in defects of Sn-doped ZnO was also interesting. The main optical defects of both Sn^{2+}- and Sn^{4+}-doped ZnO QDs changed from $V_o^{\cdot}$ defects (in ZnO QDs) to O_i and O_{Zn} defects. For Sn^{4+}, this was due to its higher charge. However, for Sn^{2+}, it was due to the change from Sn^{2+} to Sn^{4+}. The changing trends in quantum yields of Sn^{2+}-doped ZnO QDs and Sn^{4+}-doped ZnO QDs were different. For Sn^{2+}-doped ZnO QDs, not all of the Sn^{2+} transformed to Sn^{4+}, while the $V_o^{\cdot}$ defects still changed to O_i and O_{Zn} defects. As a result, the concentration of the main optical defects decreased. This made the quantum yields decrease with more Sn^{2+} doping. For Sn^{4+} doping, the main optical defects were O_i and O_{Zn} defects, with

concentrations that were proportional to the content of Sn^{4+}. As a result, the quantum yields increased with more Sn^{4+} doping.

Acknowledgements

References

1 M. S. Augustine, P. P. Jeeju, V. G. Sreevalsa and S. Jayalekshmi, *J. Phys. Chem. Solids*, 2012, **73**, 396–401.

2 Y. H. Tong, Y. C. Liu, S. X. Lu, L. Dong, S. J. Chen and Z. Y. Xiao, *J. Sol-Gel Sci. Technol.*, 2004, **30**, 157–161.

3 H.-J. Jeon, W. J. Maeng and J.-S. Park, *Ceram. Int.*, 2014, **40**, 8769–8774.

4 A. Mokhles Gerami and M. Vaez-Zadeh, *J. Supercond. Novel Magn.*, 2016, **29**, 1295–1302.

5 L.-W. Sun, H.-Q. Shi, W.-N. Li, H.-M. Xiao, S.-Y. Fu, X.-Z. Cao and Z.-X. Li, *J. Mater. Chem.*, 2012, **22**, 8221–8227.

6 Z. Chen, D. Pan, Z. Li, Z. Jiao, M. Wu, C. Shek, C. Wu and J. Lai, *Chem. Rev.*, 2014, **114**, 7442–7486.

7 C. Supatutkul, S. Pramchu, A. P. Jaroenjittichai and Y. Laosiritaworn, *Surf. Coat. Technol.*, 2016, **298**, 53–57.

8 R. Sangeetha and S. Muthukumaran, *Ceram. Int.*, 2016, **42**, 5921–5931.

9 S. J. Clark, M. D. Segall, C. J. Pickard, P. J. Hasnip, M. I. J. Probert, K. Refson and M. C. Payne, *Z. Kristallogr. - Cryst. Mater.*, 2005, **220**, 567–570.

10 J. P. Perdew, K. Burke and M. Ernzerhof, *Phys. Rev. Lett.*, 1996, **77**, 3865.

11 V. Kumar, H. C. Swart, M. Gohain, S. Som, B. C. Bezuindenhoudt and O. M. Ntwaeaborwa, *Ultrason. Sonochem.*, 2014, **21**, 1549–1556.

12 A. Khorsand Zak, W. H. Majid, H. Z. Wang, R. Yousefi, A. Moradi Golsheikh and Z. F. Ren, *Ultrason. Sonochem.*, 2013, **20**, 395–400.

13 W. Yang, L. Wang, X. Lu and Q. Zhang, *J. Mater. Sci.: Mater. Electron.*, 2015, **26**, 1113–1118.

14 W. Yang, B. Zhang, N. Ding, W. Ding, L. Wang, M. Yu and Q. Zhang, *Ultrason. Sonochem.*, 2016, **30**, 103–112.

15 W. Yang, H. Yang, W. Ding, B. Zhang, L. Zhang, L. Wang, M. Yu and Q. Zhang, *Ultrason. Sonochem.*, 2016, **33**, 106–117.

16 A. Schejn, M. Fregnaux, J. M. Commenge, L. Balan, L. Falk and R. Schneider, *Nanotechnology*, 2014, **25**, 145606.

17 H. R. Rajabi, M. Shamsipur, A. A. Khosravi, O. Khani and M. H. Yousefi, *Spectrochim. Acta, Part A*, 2013, **107**, 256–262.

18 W. Yang, L. Wang, X. Lu, Y. Ding and Q. Zhang, *Mater. Lett.*, 2015, **141**, 330–332.

19 Y. Nakanishi, K. Kato, M. Horikawa and M. Yonekura, *Thin Solid Films*, 2016, **612**, 231–236.

20 N. N. Lathiotakis, A. N. Andriotis and M. Menon, *Phys. Rev. B: Condens. Matter Mater. Phys.*, 2008, **78**, 193311.

21 S. Massidda, R. Resta, M. Posternak and A. Baldereschi, *Phys. Rev. B: Condens. Matter Mater. Phys.*, 1995, **52**, R16977–R16980.

22 R. M. Sheetz, I. Ponomareva, E. Richter, A. N. Andriotis and M. Menon, *Phys. Rev. B: Condens. Matter Mater. Phys.*, 2009, **80**, 195314.

23 B. Cao, T. Shi, S. Zheng, Y. H. Ikuhara, W. Zhou, D. Wood, M. Al-Jassim and Y. Yan, *J. Phys. Chem. C*, 2012, **116**, 5009–5013.

24 C. Chen, L. Wang, Y. Liu, Z. Chen, D. Pan, Z. Li, Z. Jiao, P. Hu, C. Shek, C. Wu, J. Lai and M. Wu, *Langmuir*, 2013, **29**, 4111–4118.

25 J. Wang, Z. Chen, Y. Liu, C. Shek, C. Wu and J. Lai, *Sol. Energy Mater. Sol. Cells*, 2014, **128**, 254–259.

26 L. Ren, D. Chen, Z. Hu, Z. Gao, Z. Luo, Z. Chen, Y. Jiang, B. Zhao, C. Wu and C. Shek, *RSC Adv.*, 2016, **6**, 82096.

27 M. Gallegos, M. Peluso, H. Thomas, L. Damonte and J. Sambeth, *J. Alloys Compd.*, 2016, **689**, 416–424.

28 B. Song, C. Ji, Y. Zhu, Z. Geng, L. Zhang, Z. Lin, C. Tuan, K. Moon and C. Wong, *Chem. Mater.*, 2016, **24**, 9110–9121.

29 B. Song, J. Zhao, M. Wang, J. Mullavey, Y. Zhu, Z. Geng and D. Chen, *Nano Energy*, 2017, **31**, 183–193.

30 J. Lin, K. Peng, H. Liao and S. Lee, *Thin Solid Films*, 2008, **16**, 5349–5354.

31 J. R. Chelikowsky, *Solid State Commun.*, 1977, **22**, 351–354.

32 A. Kobayashi, O. F. Sankey and J. D. Dow, *Phys. Rev. B: Condens. Matter Mater. Phys.*, 1983, **28**, 946–956.

33 H. Zeng, S. Yang and W. Cai, *J. Phys. Chem. C*, 2011, **115**, 5038–5043.

34 H. Fujiwara and M. Kondo, *Phys. Rev. B: Condens. Matter Mater. Phys.*, 2005, **71**, 075109.

35 B. Delley, *J. Chem. Phys.*, 2000, **113**, 7756–7764.

36 B. Delley, *J. Chem. Phys.*, 1990, **92**, 508–517.

37 K. Vanheusden, W. L. Warren, C. H. Seager, D. R. Tallant, J. A. Voigt and B. E. Gnade, *J. Appl. Phys.*, 1996, **79**, 7983–7990.

38 B. Lin, Z. Fu and Y. Jia, *Appl. Phys. Lett.*, 2001, **79**, 943.

39 H. S. Kang, J. S. Kang, J. W. Kim and S. Y. Lee, *J. Appl. Phys.*, 2004, **95**, 1246–1250.

40 J. J. Shi, S. Wang, T. T. He, E. S. Abdel-Halim and J. J. Zhu, *Ultrason. Sonochem.*, 2014, **21**, 493–498.

41 W. K. Bae, K. Char, H. Hur and S. Lee, *Chem. Mater.*, 2008, **20**, 531–539.

42 K. F. Mak, C. Lee, J. Hone, J. Shan and T. F. Heinz, *Phys. Rev. Lett.*, 2010, **105**, 136805.